SUPPLEMENTARY MATERIAL

The mechanics of snow friction as revealed by micro-scale interface observations

James H. Lever, Susan Taylor, Arnold J. Song, Zoe R. Courville,
Ross Lieblappen, Jason C. Weale

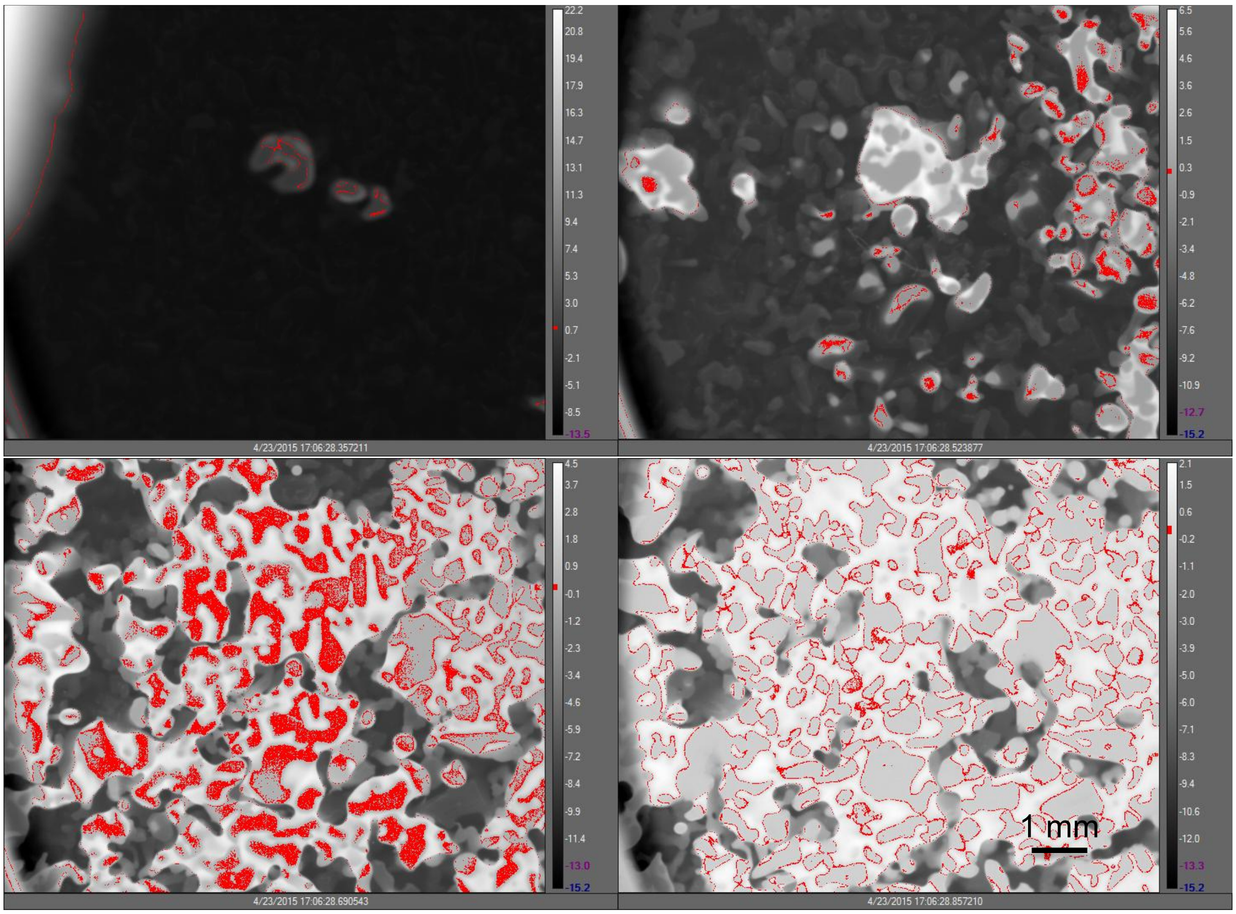

Fig. S1. Thermographs of a warm SiO_2 window placed on a snow sample. The images are five frames (0.13 s) apart selected from a 30 Hz sequence and progress left to right on upper row, then left to right on the lower row. The red pixels measure -0.1°C to 0.1°C; white pixels are warmer and grey and black ones are colder than this range. The upper-left image shows first contact between the snow and the warm window. The lower-left image shows maximum snow-grain melted area, while the lower-right image shows the refreeze front along the boundaries of the melted grains and the adjacent water. Melt water warmer than 0°C was in contact with the warm window but not the underlying snow grains.

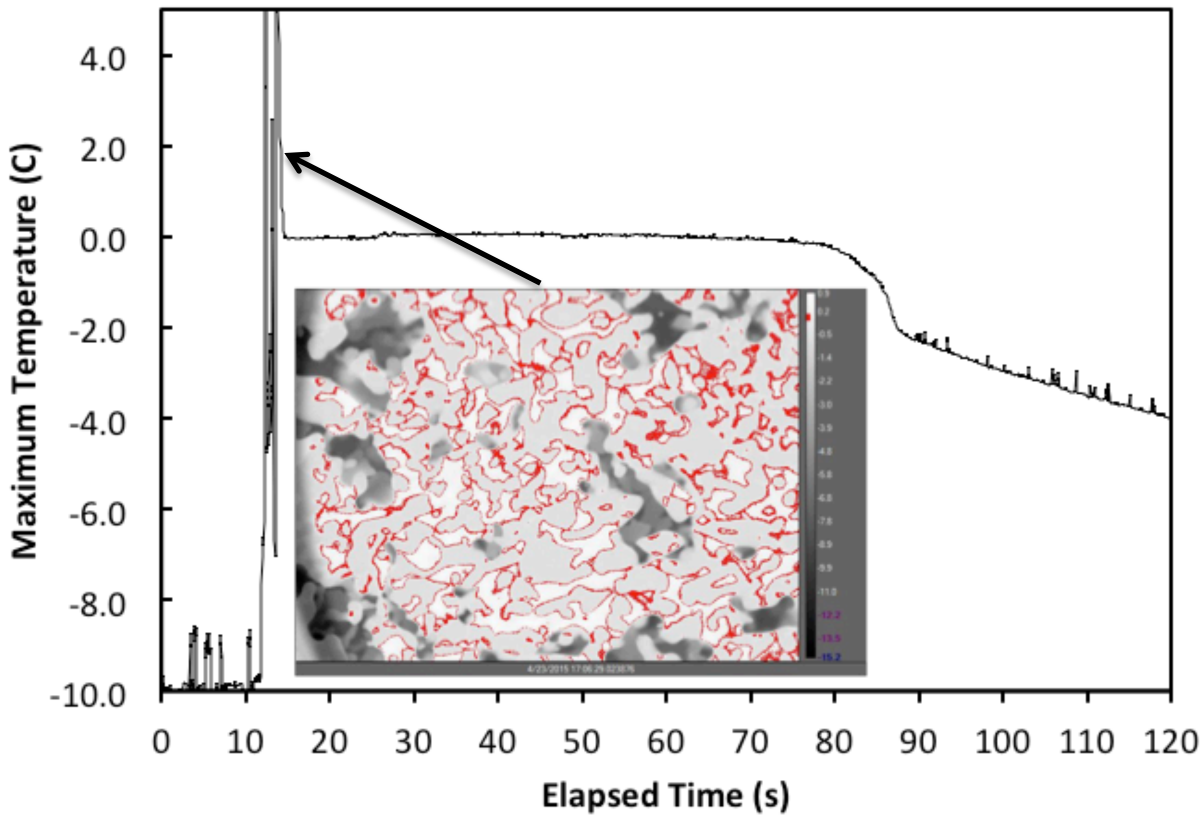

Fig. S2. Maximum surface temperature during the warm-window calibration test. The inset thermograph shows the refreeze front at 14.3 s, five frames (0.13 s) after the last image in Fig. S1. The ~ 60 s temperature plateau beginning at 14.6 s measured 0.0 ± 0.1°C, consistent with slowly refreezing melt water, and confirmed the IR camera's calibration in the temperature range of interest.

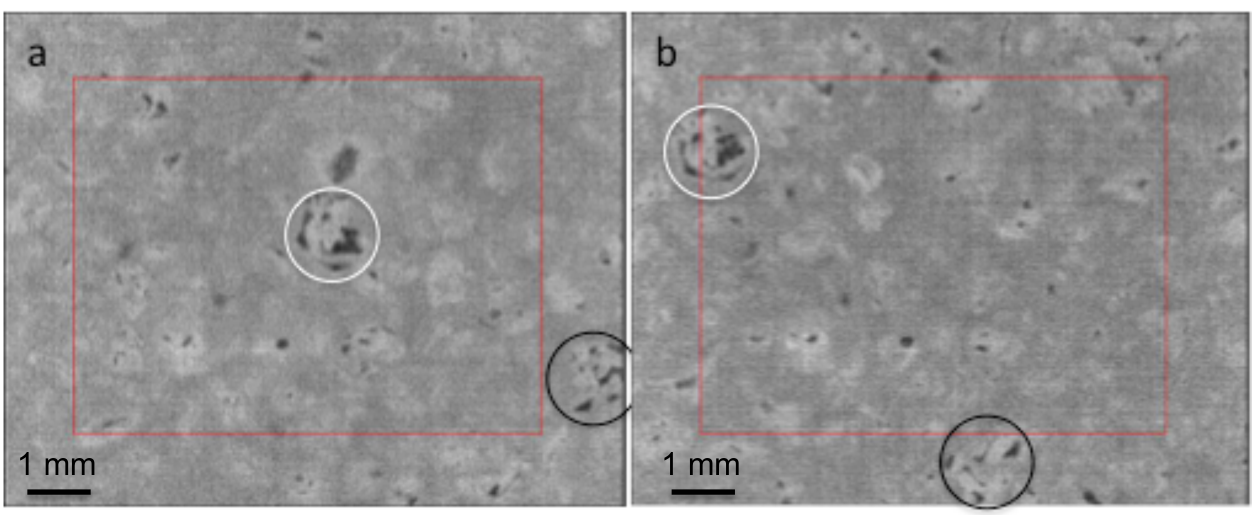

Fig. S3. Successive IR images (4 s apart) near the start of test 160603. This test produced widespread inter-granular bond failure. White pixels are warmer and black ones are colder than average. The circled features show movement of coherent clusters of snow grains and air pockets. Slider motion was from right to left. Friction coefficient ranged 0.026 – 0.032 during the test. Red box is a reference frame superimposed on the thermograph.

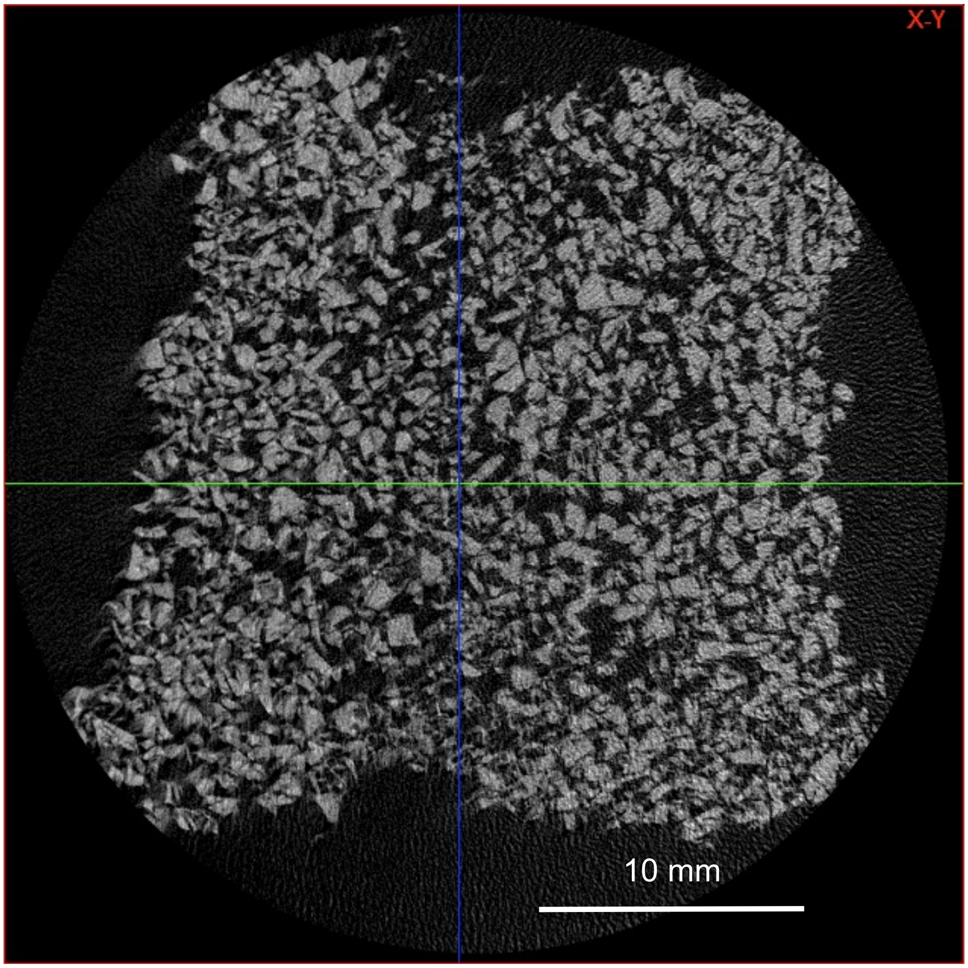

Fig. S4. Micro-CT reconstructed geometry of the glazed surface from test 160613. The 15-μm-thick horizontal slice shows snow grains in light grey and air pockets in black. The areal density in this slice is much higher ($A_r/A_n = 0.46 \pm 0.02$) than the total contact area of $A_r/A_n = 0.15 \pm 0.02$ measured using IR images owing to near-surface collections of abraded ice crystals.

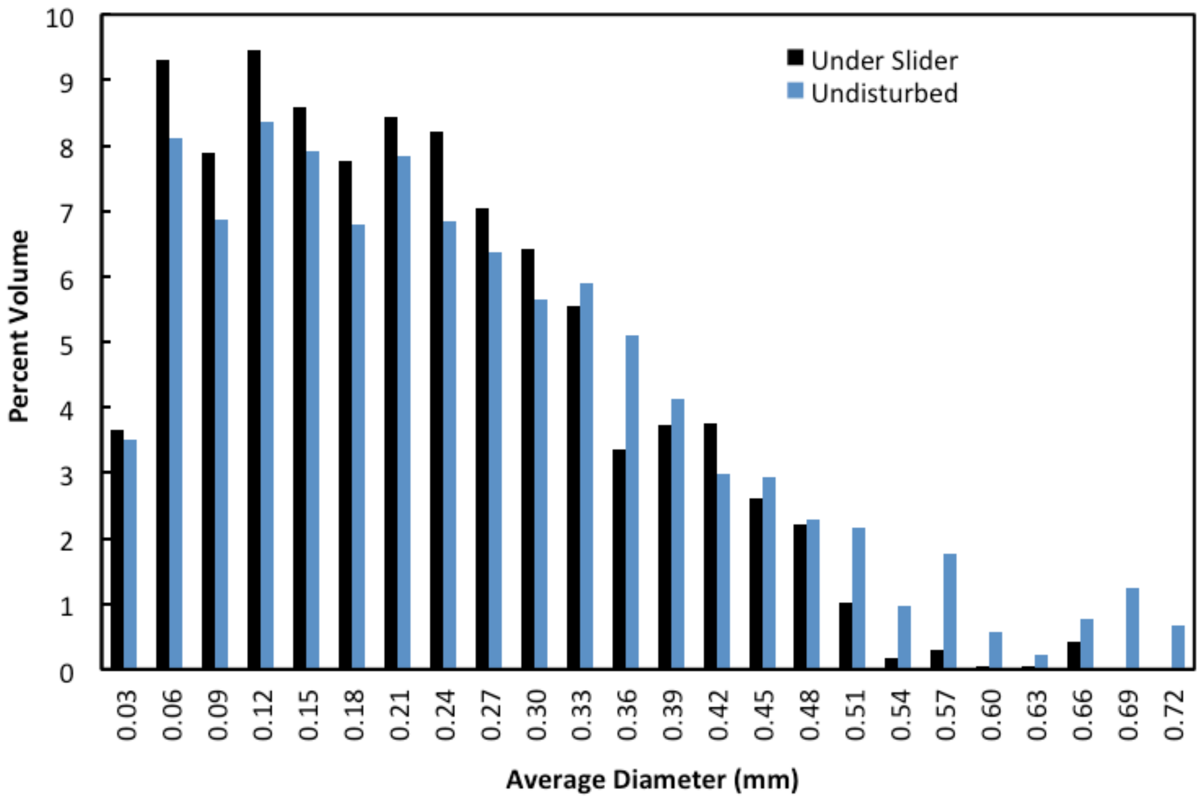

Fig. S5. Snow grain-size distribution in top 750 μm of specimen from test 160613. Snow-grain equivalent diameter was calculated from 15-μm slices through the micro-CT 3-D reconstructed geometry. While useful to characterize bulk-snow properties, the analyses did not reveal significant differences in grain-size distributions under the slider compared with undisturbed snow, because the micro-CT resolution was insufficient to image individual abraded particles that resulted from slider motion.

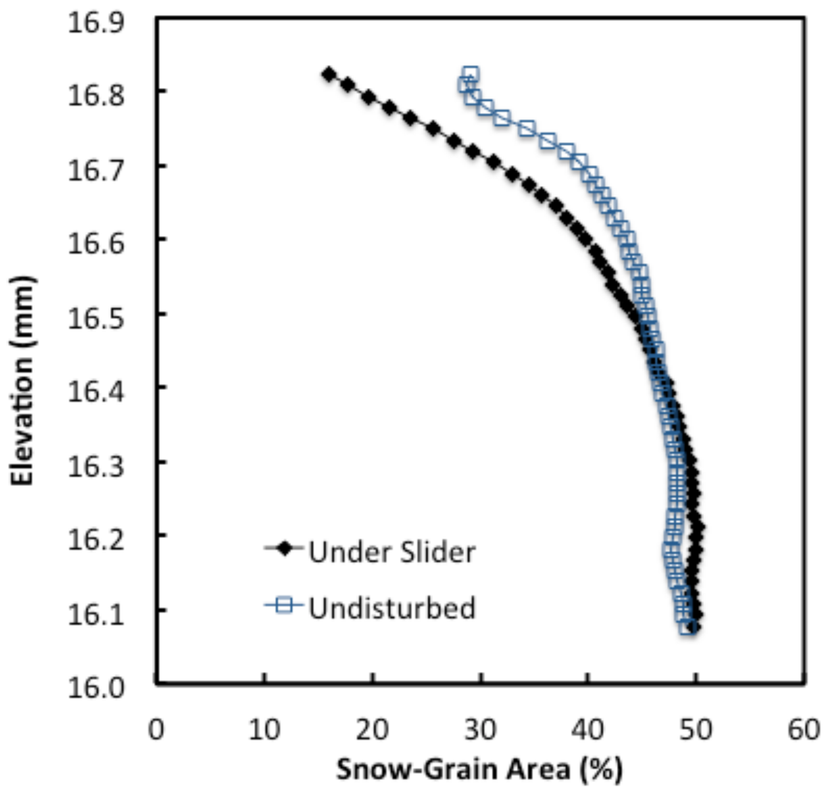

Fig. S6. Snow-grain area profile in top 750 μm of specimen from test 160613. The areal density (equivalent to volumetric density) was calculated from 15-μm slices through the micro-CT 3-D reconstructed geometry of the specimen. Loose surface grains from specimen extraction blurred the transition from air to snow under the slider. The under-slider profile showed a very slight density increase with depth before converging to the same profile as the undisturbed section. This small increase is consistent with minimal compaction of the strong snow tested. Also, the slight density increase under the slider could reflect the accumulation of abraded particles even though individual particles were not resolved.

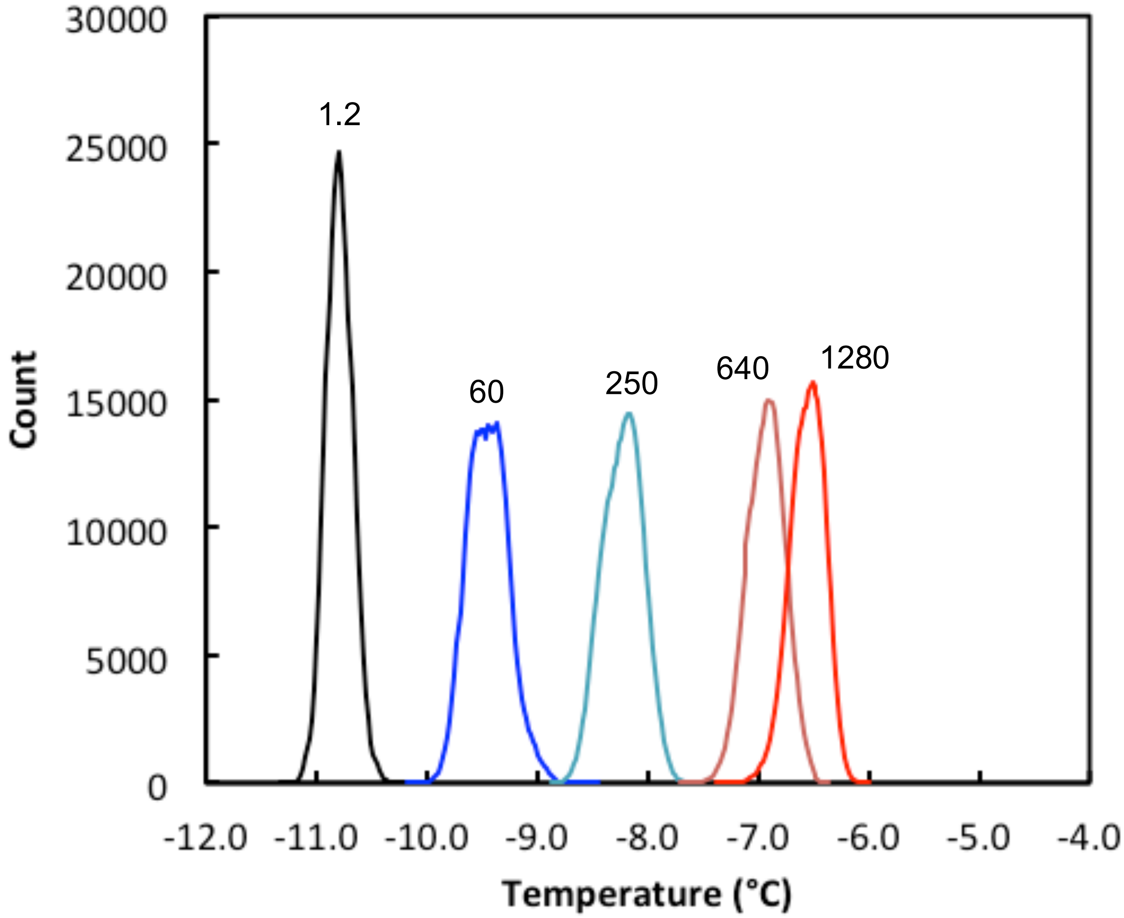

Fig. S7. Evolution of surface-temperature histograms during test on 160613. The number over each histogram is the slider-travel distance (m) at the time of the measurement. All tests with persistent contacts produced single-mode histograms. Widespread sub-pixel melting would have produced secondary, higher-temperature modes as the tests proceeded.

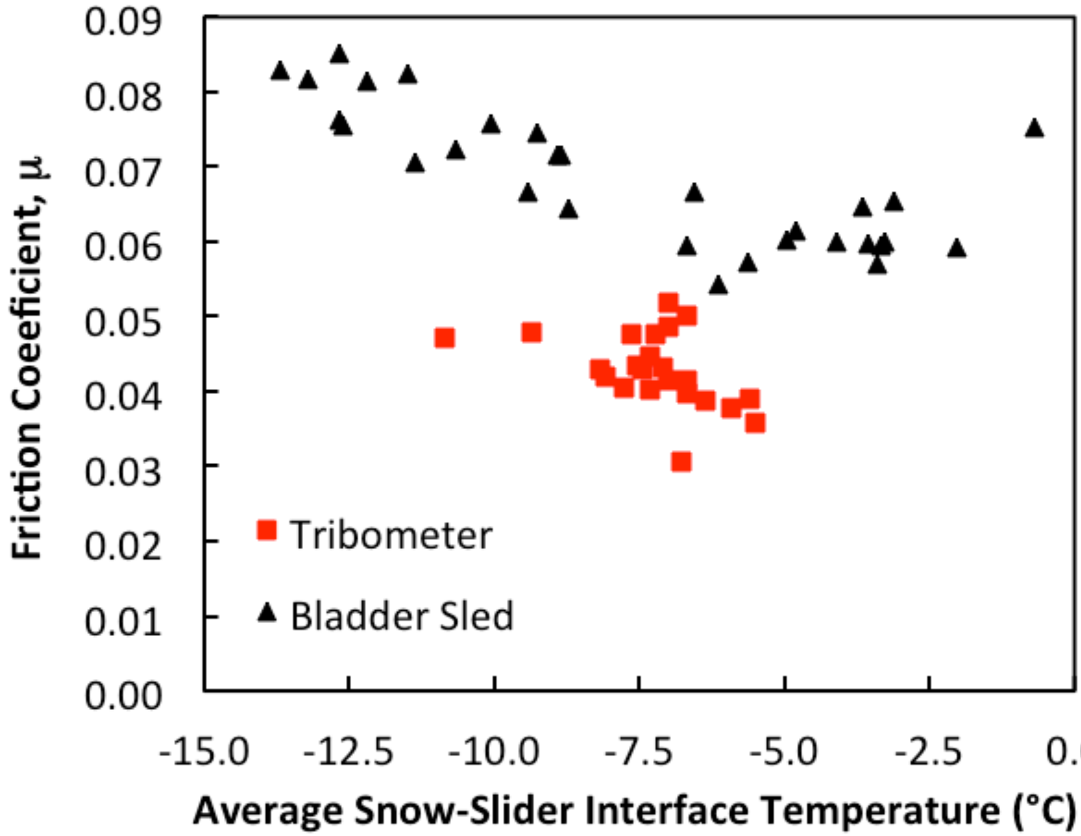

Fig. S8. Variation in friction coefficient with snow-slider interface temperature. The tribometer data are 30-s average values at the end of each speed setting for tests with persistent contacts. Bladder-sled data are steady-state values from field trials in Greenland of fuel-bladder sleds (Lever and Weale, 2012) that used various techniques to increase interface temperatures (heating blankets, sled insulation, solar gain from black covers) and let to the adoption of black fuel bladders to improve sled efficiency (Lever and others, 2016).

Effect of IR-emissions mixing with depth into a contacting snow grain

IR emissions ("heat radiation") emanate from volume elements within a material at the expense of heat energy within the elements (Planck, 1914). The surface emissions are then the net result of local emission and transmission through some depth within the body. Because slider friction produced a temperature gradient into contacting snow grains, with the surface warmer than the interior, the net IR emissions received at the camera reflected a temperature that was slightly colder than the surface temperature. We seek here to quantify this effect to determine whether the IR camera would have missed detecting 0°C has it occurred.

By Kirchhoff's Law, emissivity of a material at any wavelength equals its absorptivity at that wavelength. We may use published absorption coefficients for polycrystalline, freshwater ice to determine the depths below the surface of a snow grain from which 3 – 5 μm IR emissions would contribute to the camera measurements. For this purpose, we use the compilation of

Warren and Brandt (2008) to obtain linear absorption coefficients, $k_a(\lambda)$, for ice Ih near 0°C (Table S1), with k_a defined by the equation:

$$\frac{I}{I_0} = \exp\left(-k_a l\right) \quad \text{(S1)}$$

where I_0 and I are the radiation intensities at wavelength λ before and after travelling through ice of thickness l. The depths from which 95% of the 3 – 5 μm IR emissions reach the surface, l_{95}, are thus 1.2 – 130 μm via Equation (S1).

Table S1. Absorption coefficients $k_a(\lambda)$ (from Warren and Brandt, 2008), depth from which emissions contribute, l_{95}, fractional contribution of emissive power in 3 – 5 μm spectral range at 0°C, and emissions-weighted l_{95}.

λ (μm)	**$k_a(\lambda)$ (μm^{-1})**	**l_{95} (μm)**	**$E_b(\lambda,0°C)/\Sigma E_b(\lambda,0°C)$**	**Emissions-Weighted l_{95} (μm)**
3.0	1.72	1.7	0.002	0.0028
3.1	2.47	1.2	0.002	0.0030
3.2	1.18	2.5	0.004	0.0090
3.3	0.32	9.5	0.005	0.048
3.4	0.12	25	0.007	0.170
3.5	0.050	60	0.009	0.556
3.6	0.028	110	0.012	1.32
3.7	0.024	130	0.016	2.02
3.8	0.023	130	0.020	2.64
3.9	0.029	100	0.026	2.62
4.0	0.038	79	0.032	2.52
4.1	0.043	70	0.039	2.70
4.2	0.057	53	0.047	2.46
4.3	0.058	51	0.056	2.85
4.4	0.077	39	0.066	2.54
4.5	0.087	35	0.076	2.65
4.6	0.074	41	0.088	3.59
4.7	0.053	56	0.101	5.69
4.8	0.045	67	0.115	7.77
4.9	0.036	83	0.130	10.9
5.0	0.030	99	0.146	14.5
Average		58.9		67.6

The mixing of IR emissions is of greatest concern when the near-surface temperature gradients are largest. This condition occurred at the startup of each test and immediately after each slider-speed increase. To estimate the worst-case, near-surface temperature gradient, we may assume 1D transient heat conduction into the snow grain with an imposed step increase in surface temperature of 2°C at $t = 0$. This step increase exceeds the largest temperature increase that resulted at any slider-speed change, namely 1.6°C from startup to the first speed change of test 160613 (Table 1). Importantly, the measured increase occurred over 3.3 min rather than instantaneously, so calculated temperature gradients will be much stronger than those that occurred during the test. The solution to the step-increase, 1D transient heat conduction problem is (Carslaw and Jaeger, 1959):

$$T(z,t) = T_0 erfc\left(\frac{z}{2\sqrt{\alpha t}}\right) \qquad \text{(S2)}$$

where T_0 is the step temperature increase (2°C) over the initially uniform body temperature, z is depth into the snow grain, t is elapsed time, α is ice diffusivity (1.24×10^{-6} m^2/s, Kreith and Bohn, 1986) and *ercf* is the complementary error function. The temperature gradient within the first 130 μm is essentially linear with depth after $t = 0.1$ s, and at $t = 4$ s (time of the first IR image, taken after one slider revolution) the temperature at $z = 130$ μm is only 0.07°C lower than the surface temperature. The surface IR emissions thus derive from ice with temperatures within 0.07°C of the imposed surface temperature of 2°C.

The emissive power at wavelength λ from a blackbody, $E_b(\lambda, T)$ follows Planck's Law (Kreith and Bohn, 1986):

$$E_b(\lambda, T) = \frac{C_1}{\lambda^5 \left(e^{C_2 \lambda T} - 1\right)} \qquad \text{(S3)}$$

where T = absolute temperature, $C_1 = 3.74 \times 10^{-16}$ Wm^2, $C_2 = 1.44 \times 10^{-2}$ mK. Emissive power for a grey body such as ice follows the same spectral distribution. Because temperature gradients are small after $t = 4$ s, emissive power is linear with temperature across the depth of interest. Average emissive power thus equals the power at the average temperature, which is the power at the average depth:

$$\bar{E}_b(\lambda, T) = E_b(\lambda, \bar{T}) = E_b(\lambda, l_{95}/2) \quad \text{(S4)}$$

At each pixel, the IR camera converts the arriving emissive power over the wavelength interval 3 – 5 μm to an equivalent blackbody temperature, allowing for object emissivity and corrections for surface-reflected emissions and atmospheric emissions between the object and the lens (FLIR 2013). As noted, the emissivity of ice is high in the 3 – 5 μm spectral range (0.95 – 0.98) and effects of reflected and atmospheric emissions are small. Essentially, the camera integrates Equation S4 over the 3 – 5 μm spectral range. We do not know, however, whether the camera sums all arriving emissions equally or whether its gains vary with wavelength to account for lower emissive power at 3 μm compared with 5 μm. Table S1 provides two approaches to determine the equivalent depth at which the camera would determine the temperature of the total emissions. The linear-average l_{95} would be the depth if the camera gains compensate for lower emissive power at lower wavelengths. The emissions-weighted average l_{95} would be the depth for no gain compensation. Both values suggest $l_{95}/2 \sim 30$ μm as the depth into the ice at which the camera would determine a temperature based on arriving emissive power. After 4 s elapsed time, or one slider revolution, the corresponding temperature error would be only -0.02°C relative to the imposed surface step-increase of 2°C, and the error would decrease as time continues and the temperature gradients lessen. This error is well within the camera-calibration uncertainty of ± 0.1°C.

References

Carslaw HS and Jaeger JC (1959) *Conduction of Heat in Solids*. Second Edition, Oxford University Press, London.

FLIR (2013) *A6703sc User Manual*. FLIR Systems, Nashua, NH.

Kreith F and Bohn MS (1986) *Principles of Heat Transfer*. Fourth Edition, Harper & Row, New York.

Planck, M (1914) *The theory of heat radiation*. Authorized translation by M. Masius, P. Blakiston's Son & Co., Philadelphia.

Warren SG and Brandt RE (2008) *Optical constants of ice from the ultraviolet to the microwave: A revised compilation.* J. Geophysical Research, Vol. 113, D14220, doi:10.1029/2007JD009744.